Searching for quantum speedup in quasistatic quantum annealers

Mohammad H. Amin
D-Wave Systems Inc., 3033 Beta Avenue, Burnaby, British Columbia, Canada V5G 4M9
and Department of Physics, Simon Fraser University, Burnaby, British Columbia, Canada V5A 1S6
(Received 8 April 2015; published 19 November 2015)

We argue that a quantum annealer at very long annealing times is likely to experience a quasistatic evolution, returning a final population that is close to a Boltzmann distribution of the Hamiltonian at a single (freeze-out) point during the annealing. Such a system is expected to correlate with classical algorithms that return the same equilibrium distribution. These correlations do not mean that the evolution of the system is classical or can be simulated by these algorithms. The computation time extracted from such a distribution reflects the equilibrium behavior with no information about the underlying quantum dynamics. This makes the search for quantum speedup problematic.

DOI: 10.1103/PhysRevA.92.052323 PACS number(s): 03.67.Ac, 03.65.−w, 03.67.Lx, 42.50.Lc

Quantum annealing (QA) [1–5] is a means for solving optimization problems by using quantum mechanics. Recently, QA processors with up to more that a thousand qubits have been developed [6] and tested by many independent research groups [7–16]. The processors are designed to implement a transverse Ising Hamiltonian:

$$H(s) = -A(s)\sum_i \sigma_i^x + B(s)\mathcal{H}_P, \tag{1}$$

$$\mathcal{H}_P = \sum_i h_i\sigma_i^z + \sum_{i<j} J_{ij}\sigma_i^z\sigma_j^z, \tag{2}$$

where $\sigma_i^{x,z}$ are Pauli matrices acting on qubit i,$s = t/t_a$, t is time, t_a is the annealing time, h_i and J_{ij} are tuneable dimensionless parameters, and $A(s)$ and $B(s)$ are monotonic functions such that $A(0) \gg B(0) \approx 0$ and $B(1) \gg A(1) \approx 0$ [see Fig. 2(a)]. A successful computation yields the ground state or an acceptable low-energy eigenstate of $\mathcal{H}_P$.

By now, the presence of quantum mechanics [6,7], including entanglement [17] and the computational benefit of multiqubit tunneling [14], has been established in the QA processors. However, whether quantum mechanics can lead to any scaling advantage (quantum speedup) over available classical algorithms remains an open question. Recently, there have been many attempts to detect signatures of quantum speedup in D-Wave Two (DW2) QA processors [8–10,18]. In these studies the processor's performance is compared with some classical algorithms, such as simulated annealing (SA), quantum Monte Carlo simulation of QA (SQA), or other algorithms. The computation time t_c is typically expressed as a function of the success probability, which is usually taken to be the final ground-state probability P_0. Here, we define

$$t_c = t_a/P_0, \tag{3}$$

which is asymptotically equivalent to the definition used in previous publications [8–10,18]. For a classical solver such as SA or SQA, t_a is taken to be proportional to the number of sweeps (number of iterations in which all spins are updated in a single anneal).[1]

One hopes to determine how t_c scales with the problem size N and whether the quantum annealer provides a better scaling compared to classical solvers. For problems with essentially two-dimensional structure, such as the Chimera graph (the native graph of DW2), t_c is expected to be an exponential function of $\sqrt{N}$ (i.e., the tree width of the graph). The slope of $\log(t_c)$ versus $\sqrt{N}$, therefore, provides the coefficient in the exponent. Quantum speedup then means that the quantum annealer provides a smaller slope than other classical solvers. In practice, complications arise due to the dependence of the scaling curves on t_a. Figure 1(a) shows schematically a behavior commonly observed from some annealing algorithms, such as SA or SQA. The slope of the curves are small for small N, because t_a is typically too long for such easy problems. The slope increases abruptly at large N reflecting the fact that the chosen t_a is not long enough to find a solution. This makes the asymptotic scaling of the algorithm unclear. To deal with this problem, Ref. [8] suggests optimizing all of the annealers at each size, i.e., finding the optimal t_a that minimizes t_c for each N. The resulting "optimal" curve will be independent of a particular choice of t_a (the blue line in Fig. 1).

In practice, QA processors come with their own limitations in terms of control parameters or available annealing schedules. For example, DW2 annealing curves, $A(s)$ and $B(s)$, are fixed and the minimum available t_a is 20 μs, which is typically too long rendering suboptimal computation. In the absence of an optimal scaling, it was suggested [8,9] to determine an upper bound for quantum speedup using a suboptimal scaling. Suppose Fig. 1(a) is the t_c obtained from a quantum annealer with the minimum-allowed annealing time t_{a3} and maximum 512 qubits ($\sqrt{N} < 23$). The red curve in Fig. 1(a) represents the experimentally accessible region. It is clear that the slope of the red curve in Fig. 1(a) is not a representative of the asymptotic performance. If we were allowed to decrease t_a so that optimization becomes feasible, it would have been possible to obtain the blue (optimal) curve, which has more slope than the red one. Therefore, the slope of the measured

[1]This is $1/N$ times smaller than the total computation time if only a single-core processor is used. This factor is incorporated to include the possibility of classical parallelism (for a more detailed discussion see Ref. [14]).

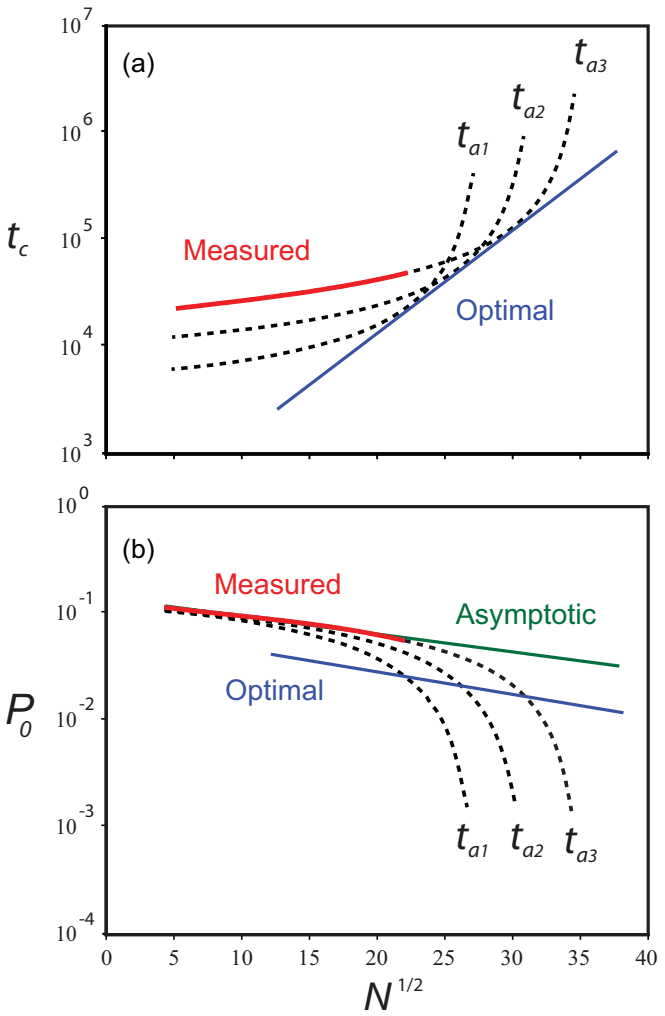

FIG. 1. (Color online) (a) A sketch of computation time as a function of $\sqrt{N}$ for different annealing times $t_{a1} < t_{a2} < t_{a3}$. Similar behavior has been observed in SA and SQA and conjectured for QA [8,9]. The blue line shows scaling of an optimized solver. The red line represents the region accessible by a quantum annealer with $t_a \geqslant t_{a3}$ and $N \leqslant 512$. (b) The success probability for the same system. The optimal curve in panel (b) is plotted by connecting the corresponding tangency points in panel (a). We have assumed $T > 0$ to correspond better with a realistic quantum annealer. At $T = 0$, the asymptotic probability is flat at $P_0 = 1$.

(red) curve provides a lower bound for that of the optimal (blue) curve.

To acquire more intuition, we plot in Fig. 1(b) the success probability P_0 by inverting each curve in Fig. 1(a) and shifting vertically (since $\log P_0 = \log t_a - \log t_c$). The curves in Fig. 1(b) tend to overlap at small N, demonstrating weak dependence of P_0 on t_a for small N (or long t_a). Such a weak dependence, commonly observed in both QA and classical algorithms, is an indication of *quasistatic* behavior. In thermodynamics, a system is called quasistatic when its time dependence is very slow compared to its relaxation time so that it stays near the equilibrium state at all times. Typically, in QA the system will follow the equilibrium distribution up to some point but then starts deviating from equilibrium and the probabilities will all freeze shortly thereafter. If the time between the deviation and freezing is short, the final probabilities will be close to the equilibrium probability distribution at a single (freeze-out) point within the freezing region. To demonstrate this behavior numerically, we consider a 16-qubit problem with h_i selected from $\pm 1/3$ and J_{ij} from $\pm 1/3$ or -1 uniform randomly. Figure 2(b) shows (solid lines) the 12 lowest-energy eigenvalues of $H(s)$ obtained with the realistic $A(s)$ and $B(s)$ plotted in Fig. 2(a). The dashed black lines represent the corresponding classical energies, i.e., eigenvalues of $B(s)\mathcal{H}_P$. We calculate the occupation probabilities by using the open quantum (Redfield) master equation discussed in Refs. [6,14,19]. Similar master equations have proven to provide good qualitative and quantitative descriptions of superconducting QA processors [6,7,11,14,20]. We assume an Ohmic environment at equilibrium temperature $T = 40$ mK with dimensionless coupling constant $\eta = 0.24$. The same model with the same parameters was successfully used to explain the experimental data in Ref. [14]. Here, we have chosen a larger than normal temperature to deliberately populate the excited states, otherwise the desired effects would not have been visible. Circles in Fig. 2(c) represent the occupation probabilities of the lowest 12 eigenstates during the evolution. We have also plotted the equilibrium probabilities (solid lines) using the Boltzmann distribution: $P_n^{\mathrm{B}}(s) = Z^{-1} e^{-E_n(s)/k_B T}$, where $E_n(s)$ is an instantaneous eigenvalue of $H(s)$, k_B is the Boltzmann constant, and $Z = \sum_n e^{-E_n(s)/k_B T}$ is the partition function. As can be seen in the figure, the probabilities closely follow $P_n^{\mathrm{B}}(s)$ up to almost 2/3 of the evolution (green region). As $s \to 1$, $A(s)$ becomes smaller, making the thermal relaxation slower. When the relaxation becomes too slow, the system stops following equilibrium and the probabilities start deviating from Boltzmann until they all saturate (freeze). The saturations happen within a freezing (yellow) region. If the freezing region is narrow enough, then the final probabilities will be close to the Boltzmann probability distribution at a single freeze-out point $s = s^*$, marked by the red vertical dotted line in Fig. 2.

Typically, s^* depends weakly on t_a. Let $\gamma(s)$ denote the dominant relaxation rate at s. As $s \to 1$, $\gamma(s)$ vanishes exponentially due to exponential decay of $A(s)$, i.e., $\gamma(s) \sim \gamma_0 e^{-\alpha s}$ where γ_0 and α are problem dependent constants. The freeze-out happens when $\gamma(s)$ becomes too small compared to t_a^{-1}, therefore no thermal transition can happen during the rest of the annealing. This mean $\gamma_0 e^{-\alpha s^*} \approx t_a^{-1}$, which yields $s^* \approx \ln(\gamma_0 t_a)/\alpha$ or $P_0(t_a) \approx P_0^{\mathrm{B}}[\ln(\gamma_0 t_a)/\alpha]$. Expanding to linear order around s^* gives

$$P_0(t_a) \sim (\kappa/\alpha) \ln(\gamma_0 t_a), \tag{4}$$

where κ is the expansion coefficient. This weak logarithmic dependence is responsible for the asymptotic behavior illustrated in Fig. 1(b).

Notice in Fig. 2(b) that the quantum energy eigenvalues (solid lines) at $s = s^*$ are not far from the classical ones (dashed lines), although earlier they were very different. The final probabilities are therefore close to a classical Boltzmann distribution, even though the dynamics during the evolution are not classical. This can explain correlations with SA as reported in, e.g., Ref. [9].

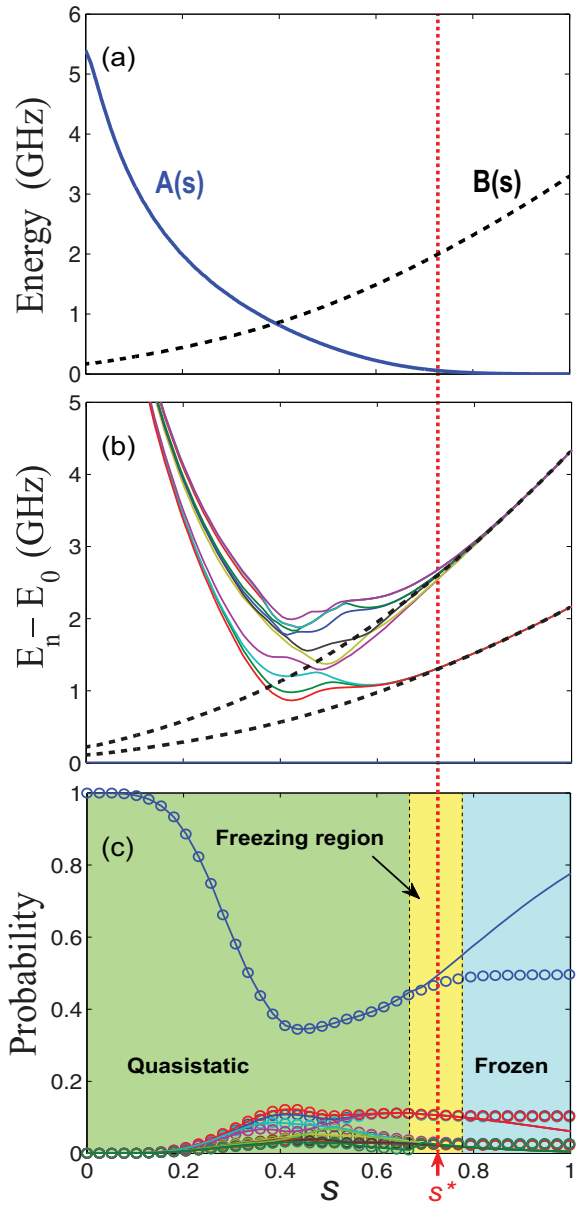

FIG. 2. (Color online) (a) Envelope functions $A(s)$ and $B(s)$ for a DW2 quantum annealer. (b) The lowest 12 energy levels of a randomly generated 16-qubit problem. Dashed black lines are classical energies. Notice that the quantum energy eigenvalues are close to the classical ones at s^*. (c) Occupation probabilities during the annealing calculated by using the Redfield formalism (circles) and the Boltzmann distribution (solid lines), assuming $T = 40$ mK and $t_a = 20\ \mu$s. All probabilities follow the Boltzmann distribution in the quasistatic region (green) until they start freezing in the freezing region (yellow) and stay constant in the frozen region (blue). All final probabilities are close to the Boltzmann probabilities at the freeze-out point s^*, marked by the vertical (red) dashed line.

It has been conjectured that QA can become advantageous over thermal annealing or SA for problems that have thin but tall barriers in their energy landscapes [4]. The reason is tunneling through such barriers becomes more efficient than thermal excitation over the barrier. This is certainly a dynamical effect and not an equilibrium property. If the source of a possible quantum speedup is dynamical, as conjectured, then searching for the speedup requires access to such dynamics. In general, an equilibrium population is only a function of the energy eigenvalues and therefore is independent of the dynamics. For a quasistatic quantum annealer with a sharp freeze-out at $s = s^*$, the final ground-state population is close to $P_0^{\mathrm{B}}(s^*)$, which is only a function of $E_n(s^*)$. It is clear that, from such probabilities, it is not possible to determine how fast the distribution is established. For example, consider a hypothetical quantum annealer that can return a Boltzmann distribution of $H(s^*)$ within a *constant* time $t_a = O(1)$ (independent of N) that is much faster than any other classical solvers and obviously scales better than all of them. Since sampling from a Boltzmann distribution is a very hard computational problem, this hypothetical quantum annealer (although it may never exist) can provide an incredible quantum speedup for such a hard problem. Nevertheless, when assessed based on a suboptimal t_c, defined in Eq. (3), it may scale worse than some optimized classical solvers, merely due to the scaling of $P_0^{\mathrm{B}}(N)$.

We can now return to our original question of whether it is possible to determine a bound for quantum speedup from suboptimal data. If the measured slope in Fig. 1(a) provides a lower bound for the optimal slope, as it appears in that figure, then one may know with certainty when quantum speedup is not possible. A measured (suboptimal) slope being larger than the classical slopes means that the optimal slope would be even larger. Therefore, the optimized QA would scale even worse and it can never be able to provide quantum speedup. On the other hand, if the measured slope is smaller than classical, then no conclusion can be made because there is always a possibility that the optimal slope be larger than classical. In other words, it is possible to "rule out" quantum speedup from a suboptimal performance, but it is not possible to prove it. Based on what we discussed before, if the suboptimal probabilities do not provide information about the quantum dynamics, then it should not be possible to even put a bound on quantum speedup, which seems to contradict the above argument. To resolve this, we notice that the situation depicted in Fig. 1(a) is based on assumptions which may not hold in general for QA. For example, it is assumed that the slope of each curve at a fixed t_a is a monotonically increasing function of N, or that t_c increases with t_a at small N, but decreases at large N. It is also assumed [implicitly in Fig. 1(a), but explicitly in Fig. 1(b)] that the probability P_0 is a monotonically increasing function of t_a. Most of these assumptions are based on observations from classical solvers such as SQA (see, e.g., supplementary information of Ref. [8]) and may even apply to most classical solvers. Establishing that they also hold in general for QA requires a proof. It is, however, possible to disprove them by a counterexample, as we do next.

As a counterexample, we examine the last assumption mentioned above, i.e., $P_0(t_a)$ is a monotonically increasing function. We calculate P_0 as a function of t_a for the 16-qubit instance of Fig. 2 by using the Redfield model that we used before with the same realistic parameters that have shown agreement with experiment [14]. Circles (squares) in Fig. 3 are results of the master equation calculations with (without) coupling to the environment. It is clear that the open system probability behaves nonmonotonically. For

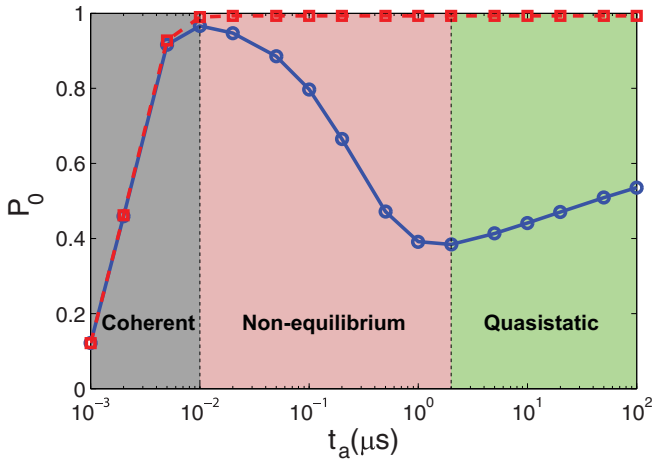

FIG. 3. (Color online) Ground-state probability as a function of t_a for the problem instance studied in Fig. 2. The circles are calculated by using the Redfield master equation calculation with the same parameters as in Fig. 2(c). The squares are results of closed-system calculations. Three regions are distinguished: *Coherent*, where the environment does not have enough time to affect the system hence the open- and closed-system probabilities coincide. *Nonequilibrium*, in which the environment starts to occupy the excited states during the evolution but does not have enough time to establish equilibrium. *Quasistatic*, where the evolution is so slow that the system follows equilibrium during most of the evolution [as in Fig. 2(c)] and P_0 depends on t_a according to Eq. (4).

short t_a, the environment does not have enough time to excite the system from the ground state; therefore, the open- and closed-system probabilities coincide (gray region). For intermediate t_a, the environment starts to populate the excited states through a nonequilibrium dynamics and the probabilities decrease (pink region). At long t_a, the system starts observing quasistatic evolution with an equilibrated final population and a P_0 that increases according to Eq. (4). Such a monotonic t_a-dependence is expected to be more generic than the chosen example. Since in QA the system starts in the ground state, the thermal excitation populates the excited states from bottom up (unlike the top-down relaxation in SA). By decreasing t_a beyond the relaxation time, the thermal processes will not have enough time to excite the system, thus P_0 will increase. When annealing becomes so fast that the nonadiabatic excitations become possible, P_0 will start decreasing again. Similar behavior has recently been observed in SQA [21].

A nonmonotonic $P_0(t_a)$ may result in a performance very different from what is predicted in Fig. 1(a). If we allow probabilities to exceed the asymptotic probability for small t_a in Fig. 1(b), then we may obtain Fig. 4(a), which leads to a t_c plotted in Fig. 4(b). The plotted optimal line in Fig. 4(b) has now a smaller slope than the asymptotic one, contradicting the argument used to bound quantum speedup. It should be emphasized that the behavior depicted in Fig. 4 serves only as a counterexample and we do not claim it to be generic for QA. Other situations may arise that could be different from both Figs. 1 and 4.

It is important to mention that the final probabilities of a quantum annealer is not always an equilibrium population,

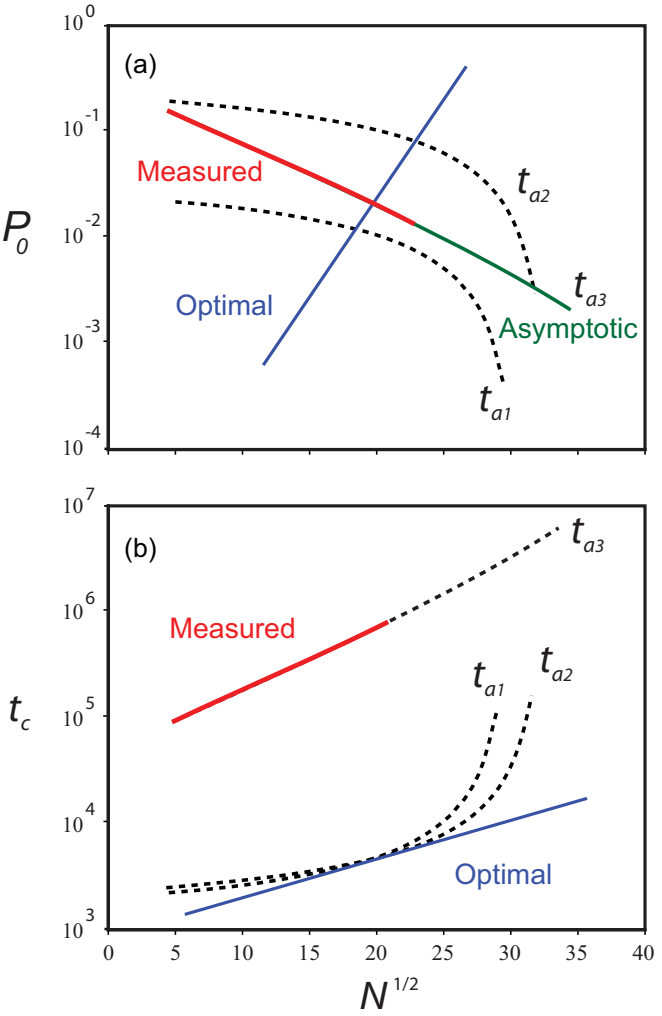

FIG. 4. (Color online) (a) P_0 and (b) t_c as a function of $\sqrt{N}$ assuming a nonmonotonic $P_0(t_a)$. The probabilities at t_{a2} exceed the asymptotic line. The optimal curve in panel (a) is plotted by connecting the corresponding tangency points in panel (b).

even for long t_a. Since the relaxation rates between different energy levels change differently with time, they may freeze at different points during the annealing, leading to a distributed freeze-out [a wide freezing region in Fig. 2(c)]. In such cases, it is not possible to identify a single freeze-out point at which the equilibrium population gives the final population. Such situations are likely to happen when the problem has a complicated energy landscape involving numerous valleys with large barriers between them. These problems are expected to have final populations that are more sensitive to t_a and do not correlate with equilibrated QMC simulations. In Ref. [22], it was shown that random problems on the Chimera graph have no spin glass phase transition at any nonzero temperature. The lack of spin-glass phase transition is an indication that the classical energy landscape of the problem is not very complex, thus equilibration may be easy. This signifies the importance of the problem selection for any exploration of the role of quantum dynamics in QA, as correctly pointed out in Ref. [22].

To summarize, we have shown that a quasistatic evolution with long annealing time can mask the underlying quantum

dynamics in a quantum annealer. The final population of such an annealer is likely to be close to a Boltzmann distribution at a single freeze-out point. It is therefore expected to correlate well with a quantum Monte Carlo simulation equilibrated at the same point with a correct temperature. Reference [12] provides indications of such correlations, although QMC was used as an annealing algorithm (SQA) with a time-dependent Hamiltonian (not at a fixed s^*), and the T used was smaller than the real temperature. This may explain why correlations did not persist when considering excited states [13]. Correlation with SA is also possible (see, e.g., Ref. [9]) but requires the quantum eigenenergies to be close to the classical energies at the freeze-out point. Other semiclassical models may also correlate with a quasistatic quantum annealer if they reach the same equilibrated population (see, e.g., Ref. [23]). These correlations are signatures of a quasistatic behavior and do not mean that the dynamics of the quantum annealer can be simulated by such algorithms. The lack of access to the relevant quantum dynamics makes the search for quantum speedup in a suboptimal quantum annealer problematic. Since one cannot neither prove nor rule out the possibility of quantum speedup, no conclusion can be made unless the optimization procedure proposed in Ref. [8] is done properly. We should emphasize that our argument does not undermine the importance of benchmarking in assessing the performance of a quantum annealer, even if suboptimal, nor do we claim that a quasistatic quantum annealer is not useful. Indeed, providing samples from a Boltzmann distribution is a very hard computational problem with many applications especially in machine learning. However, different benchmarking strategies are required to assess QA for such applications [24].

We thank T. Albash, E. Andriyash, S. Boixo, I. Hen, S. Isakov, W. Kaminsky, A. King, D. Lidar, C. McGeoch, H. Neven, J. Raymond, J. Rolfe, A. Roy, A. Smirnov, and R. de Sousa for useful discussions and comments on the manuscript.

[1] A. B. Finnila, M. A. Gomez, C. Sebenik, C. Stenson, and J. D. Doll, Chem. Phys. Lett. **219**, 343 (1994).
[2] T. Kadowaki and H. Nishimori, Phys. Rev. E **58**, 5355 (1998).
[3] G. E. Santoro, R. Martoňák, E. Tosatti, and R. Car, Science **295**, 2427 (2002).
[4] J. Brooke, D. Bitko, T. F. Rosenbaum, and G. Aeppli, Science **284**, 779 (1999).
[5] E. Farhi, J. Goldstone, S. Gutmann, J. Lapan, A. Lundgren, and D. Preda, Science **292**, 472 (2001).
[6] M. W. Johnson *et al.*, Nature (London) **473**, 194 (2011).
[7] S. Boixo, T. Albash, F. M. Spedalieri, N. Chancellor, and D. A. Lidar, Nat. Commun. **4**, 2067 (2013).
[8] T. F. Rønnow, Z. Wang, J. Job, S. Boixo, S. V. Isakov, D. Wecker, J. M. Martinis, D. A. Lidar, and M. Troyer, Science **345**, 420 (2014).
[9] I. Hen, J. Job, T. Albash, T. F. Rønnow, M. Troyer, and D. Lidar, Phys. Rev. A **92**, 042325 (2015).
[10] V. Martin-Mayor and I. Hen, Sci. Rep. **5**, 15324 (2015).
[11] W. Vinci, T. Albash, A. Mishra, P. A. Warburton, and D. A. Lidar, Phys. Rev. A **91**, 042314 (2015).
[12] S. Boixo, T. F. Rønnow, S. V. Isakov, Z. Wang, D. Wecker, D. A. Lidar, J. M. Martinis, and M. Troyer, Nat. Phys. **10**, 218 (2014).
[13] T. Albash, T. F. Rønnow, M. Troyer, and D. A. Lidar, Eur. Phys. J. Special Topics **224**, 111 (2015).
[14] S. Boixo, V. N. Smelyanskiy, A. Shabani, S. V. Isakov, M. Dykman, V. S. Denchev, M. Amin, A. Smirnov, M. Mohseni, and H. Neven, arXiv:1502.05754.
[15] A. Perdomo-Ortiz, J. Fluegemann, R. Biswas, and V. N. Smelyanskiy, arXiv:1503.01083.
[16] D. Venturelli, S. Mandra, S. Knysh, B. O'Gorman, R. Biswas, and V. Smelyanskiy, Phys. Rev. X **5**, 031040 (2015).
[17] T. Lanting *et al.*, Phys. Rev. X **4**, 021041 (2014).
[18] A. D. King, T. Lanting, and R. Harris, arXiv:1502.02098.
[19] M. H. S. Amin, C. J. S. Truncik, and D. V. Averin, Phys. Rev. A **80**, 022303 (2009).
[20] R. Harris *et al.*, Phys. Rev. B **82**, 024511 (2010).
[21] D. S. Steiger, T. F. Rønnow, and M. Troyer, arXiv:1504.07991.
[22] H. G. Katzgraber, F. Hamze, and R. S. Andrist, Phys. Rev. X **4**, 021008 (2014).
[23] S. W. Shin, G. Smith, J. A. Smolin, and U. Vazirani, arXiv:1401.7087.
[24] Some benchmarking strategies are discussed in H. G. Katzgraber, F. Hamze, Z. Zhu, A. J. Ochoa, and H. Munoz-Bauza, Phys. Rev. X **5**, 031026 (2015).